Universiteit Leiden
The Netherlands

The good? The bad? The mutant! Characterization of cancer-related somatic mutations and identification of a selectivity hotspot in adenosine receptor
Wang, X.

Version:	Publisher's Version
License:	
Downloaded from:	

Chapter 6

Cancer-related somatic mutations in transmembrane helices alter adenosine A_1 receptor pharmacology.

Abstract

Over-expression of the adenosine A_1 receptor (A_1AR) has been detected in various cancer cell lines. However, the role of A_1AR in tumor development is still unclear. Thirteen A_1AR mutations were identified in the Cancer Genome Atlas from cancer patient samples. We have investigated the pharmacology of the mutations located at the 7-transmembrane domain using a yeast system. Concentration-growth curves were obtained with the full agonist CPA and compared to the wild-type hA_1AR. H78L[3.23] and S246T[6.47] showed increased constitutive activity, while only the constitutive activity of S246T[6.47] could be reduced to wild-type levels by the inverse agonist DPCPX. Decreased constitutive activity was observed on 5 mutant receptors, among which A52V[2.47] and W188C[5.46] showed a diminished potency for CPA. Lastly, a complete loss of activation was observed in 5 mutant receptors. A selection of mutations was also investigated in a mammalian system, showing comparable effects on receptor activation as in the yeast system, except for residues pointing towards the membrane. Taken together, this study will enrich the view of receptor structure and function on A_1AR, enlightening the consequences of these mutations in cancer. Ultimately, this may provide an opportunity of precision medicine for cancer patients with pathological phenotypes involving these mutations.

Keywords: G protein-coupled receptors, adenosine A_1 receptor, cancer, mutation, yeast system

Introduction

G protein-coupled receptors (GPCRs) are the largest protein superfamily in the human genome with approximately 800 subtypes[1]. They share a characteristic structure of seven-transmembrane helices (TMs) connected by an extracellular N-terminus, three extracellular loops (ELs), three intracellular loops (ILs) and an intracellular C-terminus[2]. GPCRs are widely distributed throughout the human body and regulate various crucial cellular and physiological functions by responding to a diverse set of endogenous ligands[3]. However, their aberrant activity and expression also substantially contributes to human pathophysiology[4].

Kinases, due to their central roles in the cell cycle, have been studied as primary focus in preclinical oncology over the last two decades[5]. GPCRs, however, have been relatively under-investigated in this context, while an increasing amount of evidence shows that GPCRs act as regulators of tumor initiation and progression as well[6]. Malignant cells often hijack the normal physiological function of GPCRs to survive, invade surrounding tissue and evade the immune system[7]. Moreover, somatic mutations of GPCRs have been identified in approximately 20% of all cancers by a systematic analysis of cancer genomes[5].

The immune system plays a fundamental and essential role in the defense against cancer[8]. Adenosine, a nucleoside and derivative of ATP, has emerged as a major immune-metabolomic checkpoint in tumors[9]. Compared to healthy tissue, adenosine is accumulated over 50-fold in the hypoxic tumor environment, leading to a reduced anti-tumoral immune response[10]. Adenosine regulates various physiological effects and immune responses in cancer via adenosine receptors (ARs): the A_1, the A_{2A}, the A_{2B}, and the A_3 receptor[11]. Additionally, all ARs have been detected in different human tumor tissues[12]. Therefore, all four subtypes of ARs may regulate cancer progression in one way or another.

Growing evidence addresses the involvement of A_1AR in cancer progression, although its precise role is not well understood[13,14]. An increased expression level of the A_1AR has been detected in diverse cancer cells[15,16], where it appears to behave as both an anti- and pro-tumoral regulator in the development of different cancer types[10]. Interestingly, various single-site point mutations on A_1AR have been isolated from patients with different cancer types and collected by the TCGA Research Network (https://www.cancer.gov/tcga). Previous site-directed mutagenesis and docking studies on A_1AR have identified residues all over the protein involved in ligand recognition and/or functional activity[17,18]. Furthermore, several GPCR-conserved residues and motifs, for instance the D2.50 residue, the ionic lock, the NPxxY motif and the DRY motif, are located at 7-TM domains mediating ligand binding and signaling [19].

In this study, 13 mutations located at the 7-TM domains of the A_1AR have been selected from cancer patients using a bioinformatics approach. The effects of these

mutant receptors on constitutive receptor activity and agonist-induced activation were tested in a 'single-GPCR-one-G protein' *S. cerevisiae* strain, which has been reported to be predictive of the mammalian situation[20,21]. A selection of mutant receptors were further investigated for their effect on ligand binding and receptor activation in a mammalian system. Subsequently, we identified 2 CAMs, 5 CIMs and 6 loss-of-function mutants (LFMs) based on the pharmacological effects of these mutant receptors. Thus, cancer-related mutations within the 7-TM domain may alter the role of A_1AR in cancer progression and the efficacy of drugs targeting A_1AR as a cancer therapeutic approach.

Materials and methods

Data mining

Mutation data was downloaded from The Cancer Genome Atlas (TCGA, version August 8th 2015) by using the Firehose tool[22]. MutSig 2.0 data was extracted when available, MutSig 2CV was used in cases where the former was not available (specifically for Colon Adenocarcinoma, Acute Myeloid Leukemia, Ovarian Cerous Cystadenocarcinoma, Rectum Adenocarcinoma). Natural variance data was downloaded from Uniprot (Index of Protein Altering Variants, version November 11th 2015)[23]. Sequence data was filtered for missense somatic mutations and the A_1AR (Uniprot identifier P30542). The GPCRdb alignment tool was used to assign Ballesteros Weinstein numbers[24,25] to the positions through which a selection could be made for transmembrane domain positions.

Materials

The MMY24 strain and the *S. cerevisiae* expression vectors, the pDT-PGK plasmid and the pDT-PGK_hA$_1$AR plasmid (i.e. expressing the wild-type receptor) were kindly provided by Dr. Simon Dowell from GSK (Stevenage, UK). The pcDNA3.1(+) plasmid cloned with N-terminal 3xHA-tagged hA$_1$AR was ordered from cDNA Resource Center (Bloomsburg, USA). The QuikChange II® Site-Directed Mutagenesis Kit containing XL10-Gold ultracompetent cells was purchased from Agilent Technologies (Amstelveen, the Netherlands). The QIAprep mini plasmid purification kit and QIAGEN® plasmid midi kit were purchased from QIAGEN (Amsterdam, the Netherlands). Adenosine deaminase (ADA), 1,4-dithiothreitol (DTT), 8-cyclopentyl-1,3-dipropylxanthine (DPCPX) and 3-amino-[1,2,4]-triazole (3-AT) were purchased from Sigma-Aldrich (Zwijndrecht, the Netherlands). N^6-cyclopentyladenosine (CPA) was purchased from Santa Cruz Biotechnology (Heidelberg, Germany). Bicinchoninic acid (BCA) and BCA protein assay reagent were obtained from Pierce Chemical Company (Rockford, IL, USA). Radioligands 1,3-[^{3}H]-dipropyl-8-cyclopentylxanthine ([^{3}H]DPCPX, specific activity of 137 Ci × mmol^{-1}) and [^{35}S]-Guanosine 5'-(γ-thio) triphosphate ([^{35}S]GTPγS, a specific activity 1250 Ci × mmol^{-1}) were purchased from PerkinElmer, Inc. (Waltham, MA, USA). Rabbit anti-HA antibody (71-5500)

was purchased from Thermo Fisher Scientific (Waltham, MA, USA), while goat anti-rabbit IgG HRP was purchased from Jackson ImmunoResearch Laboratories (West Grove, PA, USA).

Generation of hA$_1$AR mutations

The plasmids carrying hA$_1$AR mutations were constructed by polymerase chain reaction (PCR) mutagenesis as previously described, using pDT-PGK_hA$_1$AR or pcDNA3.1_hA$_1$AR with N-terminal 3xHA tag as the template[17]. The QuikChange Primer Design Program of Agilent Technologies (Santa Clara, CA, USA) was used to design primers for mutant receptors and primers were purchased from Eurogentec (Maastricht, The Netherlands). All DNA sequences were verified by Sanger sequencing at LGTC (Leiden, The Netherlands).

Transformation in MMY24 S. cerevisiae strain

The plasmids, pDT-PGK_hA$_1$AR, containing either wild-type or mutated hA$_1$AR were transformed into a MMY24 *S. cerevisiae* strain following the Lithium-Acetate procedure[26].

Liquid growth assay

In order to characterize the mutant hA$_1$ARs, liquid growth assays in 96-well plates were performed to obtain concentration-growth curves as previously described[17]. Briefly, yeast cells expressing wild-type or mutant hA$_1$AR were inoculated to 1 mL selective YNB medium lacking uracil and leucine (YNB-UL) and incubated overnight at 30 °C. The overnight cultures were then diluted to 40,000 cells/ml (OD$_{600}$ ≈ 0.02) in selective medium without uracil, leucine and histidine (YNB-ULH). For the determination of constitutive activity, 50 μL yeast cells and 150 μL YNB-ULH medium containing different concentrations of 3-AT and 0.8 IU/ml ADA were then added to each well. To obtain concentration-growth curves, 2 μL various concentrations of ligands, 50 μL yeast cells and 150 μL YNB-ULH medium containing 7 mM 3-AT and 0.8 IU/ml ADA were then added to each well. After incubation at 30 °C for 35 h in a Genios plate reader (TECAN, Switzerland) with shaking 1 min at 300 rpm every 10 min, the optical density was measured at a wavelength of 595 nm, which represented the level of yeast cell growth.

Cell culture, transient transfection and membrane preparation

Chinese hamster ovary (CHO) cells were cultured at 37 °C in 5% CO$_2$ in a Dulbecco's modified Eagle's medium/Ham's F12 (1 : 1, DMEM/F12) containing 10% bovine calf serum, streptomycin (50 μg/mL) and penicillin (50 IU/mL). Cells were grown until 80-90% confluency and subcultured twice weekly.

Transient transfection of CHO cells with wild-type or mutated hA$_1$AR plasmid constructs was performed using a polyethylenimine (PEI) method[27]. Cells were seeded in 10-cm culture dishes to achieve 50-60% confluency 24 h prior to

transfection. On the day of transfection, cells were transfected with a PEI : DNA ratio of 3 : 1 and plasmid DNA amount of 10 µg/dish. 24 h post-transfection, the medium was refreshed, and 48 h after transfection, cells were collected and membranes were prepared as previously described[28]. Membranes were aliquoted in 250 or 100 µL and stored at -80 °C. Membrane protein concentrations were determined using the BCA method[29].

Enzyme-linked Immunosorbent assay

The ELISA experiments were performed with some modifications of a previously published procedure[30]. 24 h after transfection, cells were seeded in a 96-well plate with a density of 10^6 cells per well. 48 h post-transfection, the cells were fixed with 4% formaldehyde and blocked with 2% bovine serum albumin (BSA) (Sigma-Aldrich Chemie N.V., Zwijndrecht, The Netherlands) in Tris-buffered saline (TBS) for 1 h. Then, the cells were incubated with rabbit anti-HA tag primary antibody (1:2500) in TBST (0.05% Tween 20 in TBS) overnight at 4 °C. The cells were washed 3 times in TBST and incubated with the goat anti-rabbit IgG HRP secondary antibody (1:6000) for 1 hour at RT. After removing the secondary antibody and washing the cells with TBS, 3, 3',5,5'-tetramethyl-benzidine (TMB) was added and incubated for 10 minutes in the dark. The reaction was stopped with 1 M H_3PO4, and absorbance was read at 450 nm using a Wallac EnVision 2104 Multilabel reader (PerkinElmer).

Radioligand displacement assay

The displacement assays were performed as described previously[31]. Briefly, to each well the following was added: 25 µL cell membrane suspension, 25 µL of 1.6 nM radioligand [^{3}H]DPCPX, 25 µL of assay buffer (50 mM Tris-HCl, pH 7.4) and 25 µL of six increasing concentrations of DPCPX (10^{-11} to 10^{-6} M) or CPA (10^{-10} to 10^{-5} M) , all dissolved in assay buffer. Note, the quantity of cell membranes (10-25 µg) was adjusted to obtain approximately 1500 DPM assay window for each mutant. Nonspecific binding was determined in the presence of 10^{-4} M CPA and represented less than 10% of the total binding. For homologous competition assays, radioligand displacement experiments were performed in the presence of 3 different concentrations of [^{3}H]DPCPX (1.6 nM, 4.5 nM and 10 nM) as well as 6 increasing concentrations of DPCPX (10^{-11} to 10^{-6} M). Incubations were terminated after 1 h at 25 °C by rapid vacuum filtration through GF/B filter plates (PerkinElmer, Groningen, Netherlands) using a Perkin Elmer Filtermate-harvester. Afterwards, filter plates were washed ten times with ice-cold buffer (50 mM Tris-HCl, pH 7.4) and dried at 55 °C for 30 min. After addition of 25 µl per well of Microscint scintillation cocktail (PerkinElmer, Groningen, the Netherlands), the filter-bound radioactivity was measured by scintillation spectrometry in a Microbeta2® 2450 microplate counter (PerkinElmer).

[^{35}S]GTPγS binding assay

[^{35}S]GTPγS binding assays were adapted from a previously published method[31].

Membrane aliquots containing 15 μg protein were incubated with a total volume of 80 μL assay buffer (50 mM Tris-HCl buffer, 5 mM MgCl$_2$, 1 mM EDTA, 100 mM NaCl, 0.05% BSA and 1 mM DTT pH 7.4 supplemented with 10 **μ**M GDP and 10 μg saponin) and 9 increasing concentrations of CPA (10^{-11} to 10^{-6} M) or 9 increasing concentrations of DPCPX (10^{-11} to 10^{-6} M) in the presence of a fixed concentration (EC$_{80}$ for wild-type or mutant hA$_1$ARs) of CPA for 30 min at 4 °C. Then 20 μL of [^{35}S] GTP**γ**S (final concentration of 0.3 nM) was added to each well and followed by 90 min incubation at 25 °C. Incubations were terminated and filter-bound radioactivity was measured as described above.

Modelling

Structures of the A$_1$AR in the inactive (PDB: 5UEN)[32] and active (PDB: 6D9H) state[33], and the inactive state of the A$_{2A}$AR (PDB: 4EIY)[34] were retrieved from the PDB. Missing side chains and loop regions were added using the GPCR-ModSim webserver[35]. All structures were aligned to the inactive A$_1$AR, and figures were generated using the PyMOL Molecular Graphics System version 2.0 (Schrödinger, LLC., USA).

Data analysis

All experimental data were analyzed by GraphPad Prism 7.0 or 8.0 (GraphPad Software Inc., San Diego, CA, USA). Data from yeast liquid growth and [^{35}S]GTPγS binding assays were analyzed by non-linear regression using "log (agonist) vs. response (three parameters)" or "log (inhibitor) vs. response (three parameters)" to obtain potency (EC$_{50}$), inhibitory potency (IC$_{50}$) and efficacy (E$_{max}$ or I$_{max}$) values. The radioligand displacement curves were obtained from a statistically preferred one-site or two-site binding model. pK$_i$ values were calculated from pIC$_{50}$ values using the Cheng-Prusoff equation, where K$_D$ values were obtained from the homologous competition assays from this study and calculated by non-linear regression using "one site – homologous"[36].

Results

Data mining

Mutation data from cancer patient isolates were obtained by data mining the TCGA database on August 8th 2015. 27 point somatic mutations were selected from in total 48 cancer-related point mutations of hA$_1$ARs based on selected cancer types, i.e. breast invasive carcinoma, colon adenocarcinoma, lung adenocarcinoma, lung squamous cell carcinoma, lymphoid neoplasm diffuse large B-cell lymphoma and rectum adenocarcinoma. After assigning Ballesteros Weinstein numbers to the positions by using the GPCRdb alignment tool, 13 mutations located at the 7-TM domains were selected for this study (Table 1). One mutation was located at the first, two at the second, two at the third, one at the fourth, one at the fifth, two at the sixth and two at the seventh TM (Figure 1A).

Table 1. List of cancer-related somatic mutations identified from different cancer types.

Mutations	Cancer types
A20T$^{1.43}$	Colon adenocarcinoma
A52V$^{2.47}$	Breast invasive carcinoma
D55V$^{2.50}$	Breast invasive carcinoma
D55G$^{2.50}$	Colon adenocarcinoma
H78L$^{3.23}$	Lung adenocarcinoma
P86L$^{3.31}$	Rectum adenocarcinoma
R122Q$^{4.40}$	Colon adenocarcinoma
L134F$^{4.52}$	Lung squamous cell carcinoma
W188C$^{5.46}$	Colon adenocarcinoma
S246T$^{6.47}$	Breast invasive carcinoma
T257P$^{6.58}$	Lung adenocarcinoma
S267I$^{7.32}$	Colon adenocarcinoma
G279S$^{7.44}$	Colon adenocarcinoma

Constitutive activity of mutant hA$_1$ARs

To first characterize the effect of the cancer-related mutations on the constitutive activity of the receptor, i.e. activity independent from an agonist, yeast growth assays were performed in the absence of agonist. First, the optimal concentration of the histidine biosynthesis inhibitor (3-amino-1,2,4-triazole, 3-AT) for constitutive activity screening was determined in response to increasing concentrations of 3-AT (Figure 1B). Upon increasing concentrations of 3-AT, cell growth of both yeast cells transformed with plasmid with or without wild-type hA$_1$AR were decreased (Figure 1B). At a concentration of 4 mM 3-AT, the two curves showed the largest difference in yeast growth, and at this point, mutant receptors with increased constitutive activity (CAM) would show a higher growth level than wild-type hA$_1$AR, while mutant receptors with decreased constitutive activity (CIM) would show a growth level in between wild-type hA$_1$AR and empty vector. Thus, using this concentration of 3-AT provided the best window to screen for both CAMs and CIMs.

Cancer-related mutations showed various effects on the constitutive activity of the hA$_1$AR (Figure 1C). Eleven out of the thirteen mutant receptors had a decreased constitutive activity compared to the wild-type hA$_1$AR. Among them, mutant receptors A52V$^{2.47}$, D55V$^{2.50}$, R122Q$^{4.40}$, L134F$^{4.52}$, W188C$^{5.46}$ and T257P$^{6.58}$ even showed similar activities as yeast cells transformed by empty vector. In contrast, increased constitutive activity was observed on two mutant receptors, i.e. H78L$^{3.23}$ and S246T$^{6.47}$.
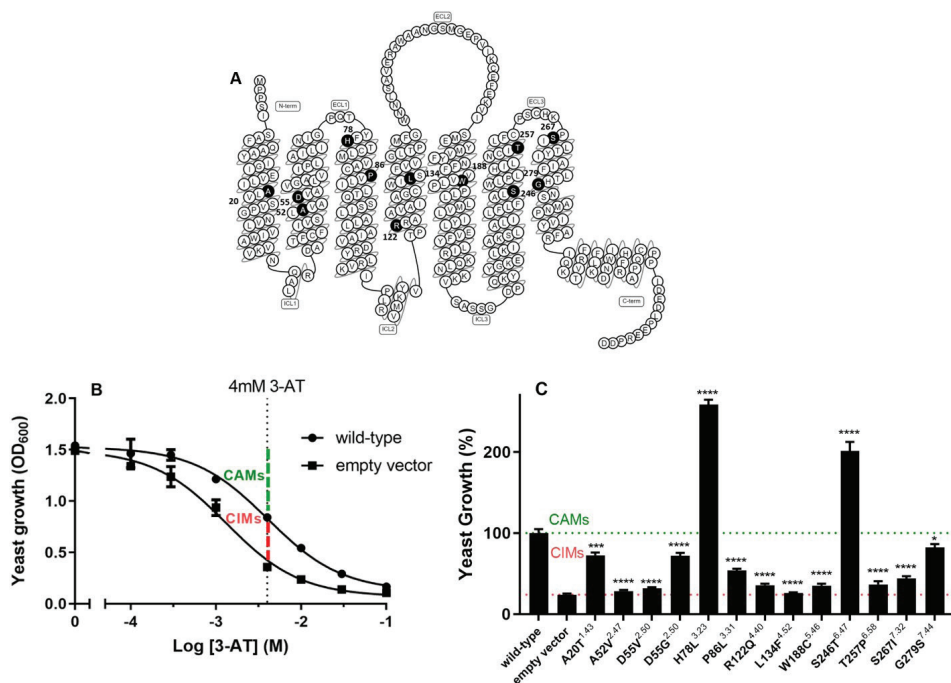
Figure 1. (A) Snake-plot of wild-type hA$_1$AR. Mutated residues are marked in black. (B) Concentration-growth curves of yeast strain in the presence or absence of wild-type hA$_1$AR. Combined graph is shown as mean ± SEM from three individual experiments performed in duplicate. (C) Constitutive activity of wild-type and 13 mutant hA$_1$ARs in the presence of 4 mM 3-AT. The yeast growth with wild-type hA$_1$AR was set to 100% and the background of the selection medium was set to 0%. The bar graph is the combined result of three independent experiments performed in quadruplicate.
* $p < 0.05$; *** $p < 0.001$; **** $p < 0.0001$ compared to wild-type hA$_1$AR, determined by using one-way ANOVA with Dunnett's post-test.
CAM: constitutively active mutant, CIM: constitutively inactive mutant

Agonist-induced receptor activation of mutant hA$_1$ARs

To further characterize the activation profiles of these mutations, concentration-growth curves were determined in the presence of increasing concentrations of the selective hA$_1$AR full agonist, CPA (Figure 2 and Table 2). Wild-type hA$_1$AR showed a potency/pEC$_{50}$ value of 9.30 ± 0.08 and a maximum effect/E$_{max}$ value (ratio over wild-type basal activity) of 4.83 ± 0.30 in the yeast system (Table 2).

Almost half of the mutant receptors with decreased constitutive activity could not be activated by CPA anymore, namely D55V$^{2.50}$, D55G$^{2.50}$, P86L$^{3.31}$, L134F$^{4.52}$, T257P$^{6.58}$ and S246I$^{7.32}$, which resulted in typing them as loss of function mutants (Figure 2 and Table 2). Other mutant receptors with decreased constitutive activity could still be activated by CPA with equal or lower potency and efficacy values. Specifically, in response to CPA, mutant receptors A20T$^{1.43}$, R122Q$^{4.40}$ and G279S$^{7.44}$ were activated to a similar activation level as wild-type hA$_1$AR with pEC$_{50}$ values of 9.24 ± 0.08, 9.04

± 0.14 and 9.27 ± 0.09, which were also not significantly different from the pEC_{50} value of the wild-type receptor. Mutant receptor A52V[2.47] had a much lower efficacy (1.86 ± 0.14) in the presence of 1 µM of CPA than wild-type hA_1AR, and also showed a more than 400-fold decreased potency. The activation level of mutant receptor W188C[5.46] was similar to wild-type hA_1AR (4.35 ± 0.10), while the potency of CPA was decreased by 10-fold.

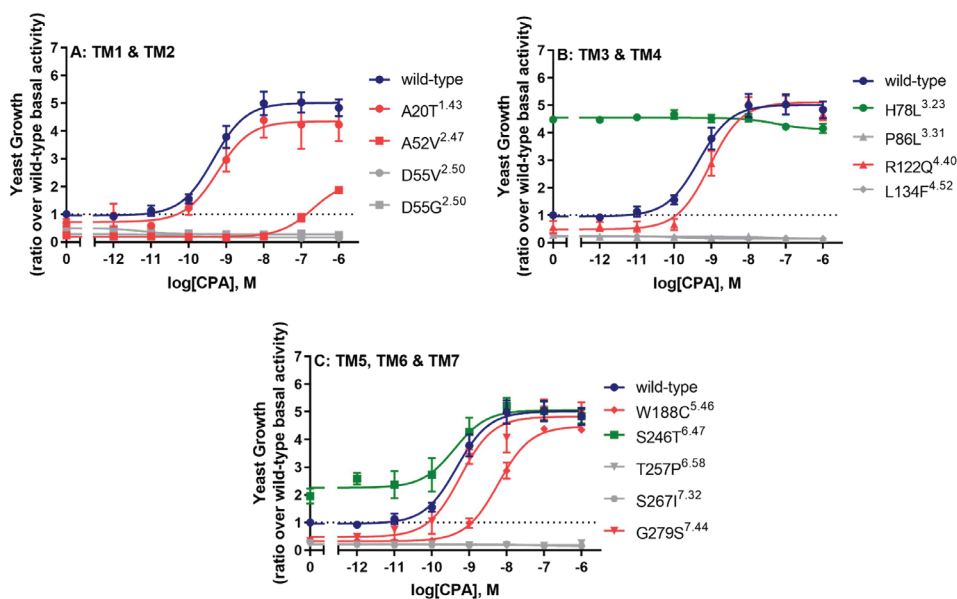The two mutant receptors with increased constitutive activity, namely H78L[3.23]

Figure 2. Concentration-response curves of wild-type and mutated hA_1ARs. Data is separated for mutations located on (A) 1st and 2nd transmembrane helix, (B) 3rd and 4th transmembrane helix and (C) 5th, 6th and 7th transmembrane helix. Data were normalized as ratio over basal activity of wild-type hA_1AR (dotted line). Combined graphs are shown as mean ± SEM from at least three individual experiments performed in duplicate. Data for wild-type is shown in dark blue, for CIMs in red, for CAMs in green and for LFMs in grey.
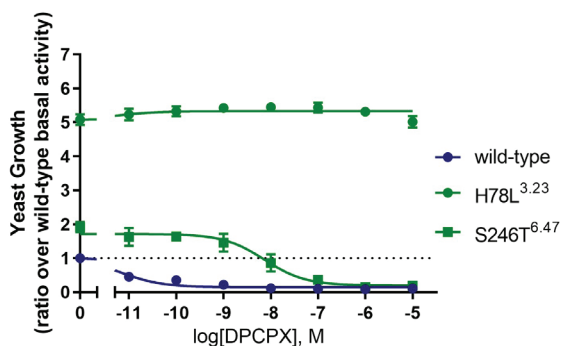

Figure 3. Concentration-inhibition curves of the hA_1AR inverse agonist DPCPX at the wild-type A_1AR and the CAMs, H78L[3.23] and S246T[6.47]. Data were normalized as ratio over basal activity of wild-type hA_1AR (dotted line). Combined graphs are shown as mean ± SEM from at least three individual experiments performed in duplicate. Data for wild-type is shown in dark blue and for CAMs in green.

and S246T$^{6.47}$, also showed increased constitutive activity in concentration-growth curves. In response to CPA, mutant receptor S246T$^{6.47}$ was activated to a similar E$_{max}$ level (4.81 ± 0.26) with a similar pEC$_{50}$ value for CPA (9.42 ± 0.33) as at the wild-type hA$_1$AR (Figure 2C and Table 2). Interestingly, mutant receptor H78L$^{3.23}$ showed a 4.5-fold increase in constitutive activity compared to wild-type, where further activation could not be obtained anymore by addition of CPA (Figure 2B and Table 2).

Next, we investigated whether the increased constitutive activity of these two mutants could be decreased using an inverse agonist, DPCPX (Figure 3). For mutant receptor S246T$^{6.47}$, DPCPX reduced the constitutive activity to wild-type hA$_1$AR levels with a pIC$_{50}$ value of 8.55 ± 0.25. However, the high constitutive activity of mutant receptor H78L$^{3.23}$ was not reduced by DPCPX.

Evaluating the diverse pharmacological effects of these mutant receptors, we characterized mutant receptors H78L$^{3.23}$ and S246T$^{6.47}$ as CAMs, mutant receptors A20T$^{1.43}$, A52V$^{2.47}$, R122Q$^{4.40}$, W188C$^{5.46}$ and G279S$^{7.44}$ as CIMs and mutant receptors D55V$^{2.50}$, D55G$^{2.50}$, P86L$^{3.31}$, L134F$^{4.52}$, T257P$^{6.58}$ and S267I$^{7.32}$ as loss of function

6

Table 2. Agonist (CPA)-induced receptor activation of wild-type and mutant hA$_1$ARs in yeast liquid growth assays.

Mutation	Basal[a]	pEC$_{50}$ (-log M)	E$_{max}$[a]	Type[b]
Wild-type	1.00 ± 0.08	9.30 ± 0.08	4.83 ± 0.30	-
A20T$^{1.43}$	0.68 ± 0.14	9.24 ± 0.08	4.23 ± 0.60	CIM
A52V$^{2.47}$	0.24 ± 0.02[***]	6.68 ± 0.09[****]	1.86 ± 0.14[**]	CIM
D55V$^{2.50}$	0.24 ± 0.04[***]	ND	ND	LFM
D55G$^{2.50}$	0.50 ± 0.06[**]	ND	ND	LFM
H78L$^{3.23}$	4.48 ± 0.12[****]	ND	4.15 ± 0.17	CAM
P86L$^{3.31}$	0.28 ± 0.03[**]	ND	ND	LFM
R122Q$^{4.40}$	0.57 ± 0.22	9.04 ± 0.14	4.67 ± 0.22	CIM
L134F$^{4.52}$	0.29 ± 0.04[**]	ND	ND	LFM
W188C$^{5.46}$	0.32 ± 0.02[**]	8.21 ± 0.10[**]	4.35 ± 0.10	CIM
S246T$^{6.47}$	1.95 ± 0.27[*]	9.42 ± 0.33	4.81 ± 0.26	CAM
T257P$^{6.58}$	0.24 ± 0.01[*]	ND	ND	LFM
S267I$^{7.32}$	0.28 ± 0.01[*]	ND	ND	LFM
G279S$^{7.44}$	0.33 ± 0.12[*]	9.27 ± 0.09	4.96 ± 0.38	CIM

Mutations are indicated using the numbering of the hA$_1$AR amino acid sequence as well according to the Ballesteros and Weinstein GPCR numbering system[24]. All values are shown as mean ± SEM obtained from at least three individual experiments performed in duplicate.
[a] Values were calculated as ratio over basal activity of wild-type hA$_1$AR.
[b] Typing of the mutants was done according to their constitutive (in)activity and agonist-induced receptor activation.
[**] $p < 0.01$; [***] $p < 0.001$; [****] $p < 0.0001$ compared to wild-type hA$_1$AR, determined by a two-tailed unpaired Student's t-test.
ND: not detectable, CAM: constitutively active mutant, CIM: constitutively inactive mutant, LFM: loss of function mutant

mutants (LFMs) (Table 2).

Ligand binding on wild-type and mutant hA$_1$ARs

Selected mutants with diverse effects on receptor activation, i.e. H78L[3.23], L134F[4.52], W188C[5.46], S246T[6.47] and G279S[7.44], were further investigated on ligand binding in a mammalian expression system. Wild-type and mutant receptors were transiently transfected into Chinese Hamster Ovary (CHO) cells, and receptor expression levels were measured by ELISA. All mutant receptors were expressed on the cell surface with similar levels to the wild-type hA$_1$AR (Figure 4A).

Affinity values of the radioligand [³H]DPCPX and B$_{max}$ values of wild-type and mutant hA$_1$ARs were determined by homologous competition displacement assays on transiently transfected membranes (Figure 4 and Table 3). [³H]DPCPX had a pK$_D$ value of 8.36 ± 0.03 at the wild-type hA$_1$AR, which was significantly higher than the value on LFM L134F[4.52] (8.06 ± 0.08), but lower than the value on CIM G279S[7.44] (8.62 ± 0.06, Table 3). Mutant receptors H78L[3.23], W188C[5.46] and S246T[6.47] showed similar pK$_D$ values of [³H]DPCPX compared to the wild-type hA$_1$AR. Diverse B$_{max}$ values were obtained on mutant receptors in comparison to wild-type hA$_1$AR (1.18 ± 0.14 pmol/mg). A significantly increased expression level of 3.74 ± 0.65 pmol/mg was observed on LFM L134F[4.52], while expression levels of CAMs H78L[3.23] and S246T[6.47] were decreased (0.17 ± 0.01 pmol/mg and 0.11 ± 0.01 pmol/mg). Note that these values did not correlate with the cell surface expression data obtained from ELISA.

Heterologous displacement by CPA of [³H]DPCPX radioligand binding on all mutant receptors as well as wild-type hA$_1$AR, was best fitted to a two-site model (Figure 4C and Table 3). Wild-type hA$_1$AR had a pK$_i$ value of 9.24 ± 0.26 for the high affinity state, 6.76 ± 0.05 for the low affinity state with a fraction value of 0.15 ± 0.03 for the high affinity state. Decreased pK$_i$ values were observed on CIM W188C[5.46] for both high and low affinity states (8.02 ± 0.16 at high affinity state and 6.15 ± 0.01 at low affinity state). LFM L134F[4.52] also showed a decreased affinity value of 6.26 ± 0.11 at the low affinity state compared to wild-type receptor, while the high affinity state was unchanged. Lastly, CAM S246T[6.47] had an increased affinity value of 7.19 ± 0.08 at the low affinity state with an unaffected affinity on the high affinity state.

[³⁵S]GTPγS functional assay on wild-type and mutant hA$_1$ARs

CHO cell membranes transiently transfected with wild-type and mutant hA$_1$AR were further tested in a functional assay, i.e. GTPγS binding (Figure 5 and Table 4). All selected mutant receptors showed a similar basal activity to wild-type hA$_1$AR. In response to CPA wild-type hA$_1$AR showed a potency/pEC$_{50}$ value of 8.98 ± 0.08 and an E$_{max}$ value (ratio over wild-type basal activity) of 1.48 ± 0.13. Only CIM W188C[5.46] showed altered receptor pharmacology upon activation by CPA with a decreased potency value of 8.28 ± 0.10, while the efficacy was not significantly affected. While
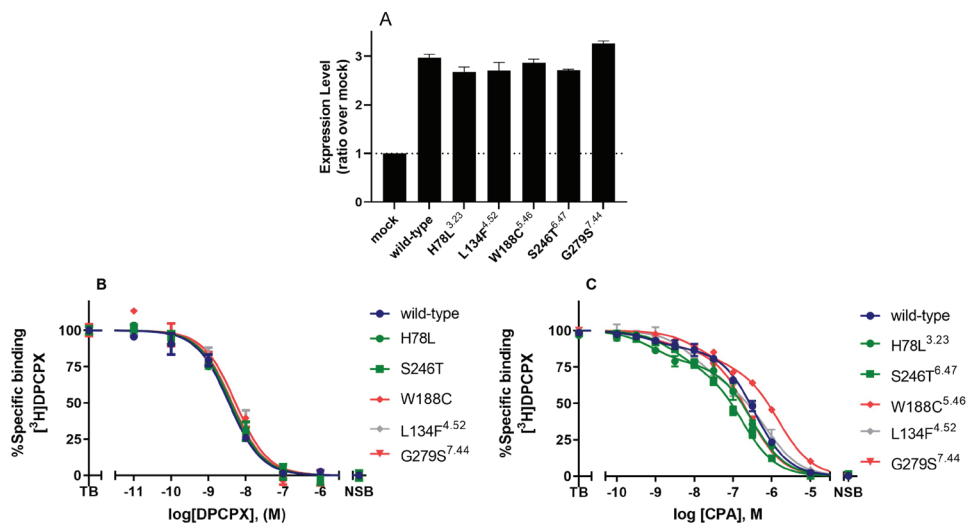
Figure 4. (A) Cell surface expression levels of wild-type and mutant hA$_1$AR transiently transfected on CHO cell membranes, as determined by ELISA. Data were normalized as ratio over mock transfected CHO cells (mock, dotted line) and shown as mean ± SEM obtained from three individual experiments performed in pentaplicate. (B and C) Displacement of specific [^{3}H]DPCPX binding to the transiently transfected wild-type hA$_1$AR, LFM L134F$^{4.52}$, CIMs W188C$^{5.46}$ and G279S$^{7.44}$, and CAMs H78L$^{3.23}$ and S246T$^{6.47}$ on CHO cell membranes by DPCPX and CPA, respectively. Combined graphs are shown as mean ± SEM from three individual experiments, each performed in duplicate. Data for wild-type is shown in dark blue, for CIMs shown in red, for CAMs in green and for LFMs in grey.
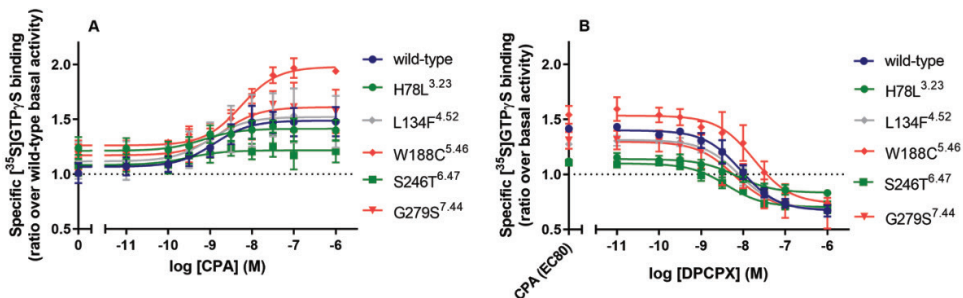

Figure 5. [^{35}S]GTPγS binding to the transiently transfected wild-type hA$_1$AR, LFM L134F$^{4.52}$, CIMs W188C$^{5.46}$ and G279S$^{7.44}$, and CAMs H78L$^{3.23}$ and S246T$^{6.47}$ on CHO cell membranes. (A) Receptor activation of wild-type and mutant hA$_1$ARs stimulated by CPA. Data were normalized as ratio over basal activity of wild-type hA$_1$AR. (B) Concentration-inhibition curves of DPCPX with the presence of CPA at the concentration of EC$_{80}$ for wild-type and mutant hA$_1$AR. Data were normalized as ratio over basal activity of wild-type or mutant hA$_1$AR. Data were obtained from three different experiments each performed in duplicate. Data for CIMs are shown in red, for CAMs in green and for LFMs in grey.

LFM L134F$^{4.52}$ did not show any activation in the yeast system, it could be activated in the mammalian system with similar potency and efficacy values for CPA compared to wild-type. CAM S246T$^{6.47}$ showed an altered receptor pharmacology upon CPA-

mediated activation with a higher pEC_{50} value of 9.44 ± 0.22 and slightly lower efficacy value of 1.21 ± 0.10 than wild-type hA_1AR, albeit not significantly different. CIM $G279S^{7.44}$ did not show a significantly different receptor pharmacology to wild-type hA_1AR in the mammalian system. Next, we investigated whether the agonist-mediated activation could be inhibited by the antagonist, DPCPX, on wild-type and mutant receptors (Figure 5B). For the wild-type receptor, the activation level was reduced to 0.67 ± 0.05 with a pIC_{50} value of 8.09 ± 0.16 for DPCPX. In the mammalian system, the CPA-mediated activation for all mutant receptors was reduced to wild-type levels with similar pIC_{50} values (Table 4).

Table 3. Affinity and B_{max} values of $[^3H]DPCPX$ and binding affinity of CPA on wild-type and mutant hA_1ARs.

	$[^3H]DPCPX^a$		CPA		
	pK_D	B_{max} (pmol/mg)	pK_i (high)	pK_i (low)	Fraction (high)
Wild-type	8.36 ± 0.03	1.81 ± 0.14	9.24 ± 0.26	6.76 ± 0.05	0.15 ± 0.03
$H78L^{3.23}$	8.46 ± 0.03	$0.17 \pm 0.01^{**}$	8.97 ± 0.35	6.83 ± 0.09	0.33 ± 0.04
$L134F^{4.52}$	$8.06 \pm 0.08^{**}$	$3.74 \pm 0.65^{**}$	8.38 ± 0.29	$6.26 \pm 0.11^{**}$	0.34 ± 0.03
$W188C^{5.46}$	8.42 ± 0.03	1.87 ± 0.12	$8.02 \pm 0.16^{*}$	$6.15 \pm 0.01^{***}$	0.29 ± 0.01
$S246T^{6.47}$	8.44 ± 0.05	$0.11 \pm 0.01^{**}$	8.98 ± 0.16	$7.19 \pm 0.08^{**}$	0.26 ± 0.03
$G279S^{7.44}$	$8.62 \pm 0.06^{*}$	2.11 ± 0.07	8.74 ± 0.48	6.78 ± 0.06	0.17 ± 0.04

All values are shown as mean ± SEM obtained from at least three individual experiments performed in duplicate.
[a] Values obtained from homologous displacement of ~1.6, 4.5 and 10 nM $[^3H]DPCPX$ from transiently transfected wild-type and mutant $CHO-hA_1AR$ membranes at 25°C.
[*] $p < 0.05$; [**] $p < 0.01$; [***] $p < 0.001$ compared to wild-type hA_1AR, determined by one-way ANOVA with Dunnett's post-test.

Table 4. Potency and efficacy values of CPA and DPCPX in $[^{35}S]GTP\gamma S$ binding assays on wild-type and mutant hA_1ARs.

	CPA			DPCPX	
	$Basal^a$	pEC_{50}	$E_{max}^{\ a}$	pIC_{50}	$I_{max}^{\ b}$
Wild-type	1.00 ± 0.09	8.98 ± 0.08	1.48 ± 0.13	8.09 ± 0.16	0.67 ± 0.05
$H78L^{3.23}$	1.24 ± 0.10	9.09 ± 0.12	1.40 ± 0.10	8.19 ± 0.25	0.83 ± 0.03
$L134F^{4.52}$	1.12 ± 0.17	9.08 ± 0.16	1.48 ± 0.24	8.14 ± 0.23	0.68 ± 0.01
$W188C^{5.46}$	1.21 ± 0.06	$8.28 \pm 0.10^{*}$	1.94 ± 0.02	7.87 ± 0.25	0.74 ± 0.03
$S246T^{6.47}$	1.08 ± 0.10	9.44 ± 0.22	1.21 ± 0.10	8.44 ± 0.10	0.70 ± 0.05
$G279S^{7.44}$	1.17 ± 0.13	8.69 ± 0.10	1.57 ± 0.20	8.23 ± 0.06	0.65 ± 0.08

All values are shown as mean ± SEM obtained from at least three individual experiments performed in duplicate.
[a] Values were calculated as ratio over basal activity of wild-type hA_1AR.
[b] Values were calculated as ratio over basal activity of wild-type or mutant hA_1AR.
[*] $p < 0.05$ compared to wild-type hA_1AR, determined by one-way ANOVA with Dunnett's post-test.

Structural mapping and bioinformatics analysis of mutations

The mutations investigated in this study were mapped on the inactive (5UEN) and active (6D9H) hA$_1$AR structure to provide structural hypotheses for the observed pharmacological effects (i.e. CIM, CAM and LFM) of the different mutations, and explain differences between yeast and mammalian data. Mutations were found scattered over the receptor structure, with LFMs indicated in black, CIMs in red, and CAMs in green (Figure 6A). Whilst some LFMs can be considered drastic changes (for instance T257P$^{6.58}$ and P86L$^{3.31}$), others are relatively mild from a structural perspective (e.g. S267I$^{7.32}$). LFMs D55V/G$^{2.50}$ sit in the sodium ion binding pocket in direct contact with the sodium ion (Figure 6B). The CAM S246T$^{6.47}$ is found near the middle of helix 6, which undergoes a large conformational change upon receptor activation (Figure 6C). Finally, W188C$^{5.46}$ and L134F$^{4.52}$ are positioned closely to one another and point towards the membrane.

6

Discussion

Although the role of hA$_1$AR in cancer progression still remains unclear, a growing amount of studies suggest that hA$_1$AR is involved in cancer development[13,14]. Previous structural studies and crystal structures of hA$_1$AR provided us with information on crucial residues for ligand binding and receptor activation, as well as essential interactions in the inactive receptor state and in G protein coupling[17,32,33,37]. Therefore, in this study we studied 13 single-site point mutations located at the 7-TM domains of A$_1$AR obtained from The Cancer Genome Atlas (TCGA). All mutations were examined in the *S. cerevisiae* system and a selection of mutations were further investigated in the mammalian system to improve our understanding of the mechanism of receptor activation with respect to cancer development and progression.

Mutations located at the top part of receptor

Mutant receptors H78L$^{3.23}$, P86L$^{3.31}$, T257P$^{6.58}$ and S267I$^{7.32}$, located at the top, extracellular part of the receptor, all showed dramatic changes upon receptor activation in the yeast system. Mutant receptor H78L$^{3.23}$ showed an extremely high constitutive activity, which could not be further induced by CPA or reduced by DPCPX (Figure 2C, 3 and Table 2). Although this could not be confirmed in the mammalian system (probably due to its low expression level), it indicates that H78L$^{3.23}$-hA$_1$AR is locked in an active conformation, which has been described previously on mutant receptor G14T$^{1.37}$ in hA$_1$AR[31]. Similar expression levels were not observed in between ELISA and homologous competition assays (Figure 4A and Table 3) due to different experimental setups that whole cell expression of functioning receptors were determined in homologous competition assays[38]. Crystallographic structural evidence of the inactive-state A$_1$AR reveals that H78$^{3.23}$ forms a salt bridge with E164, which is important for the stabilization of a β-sheet between EL1 and EL2[32].
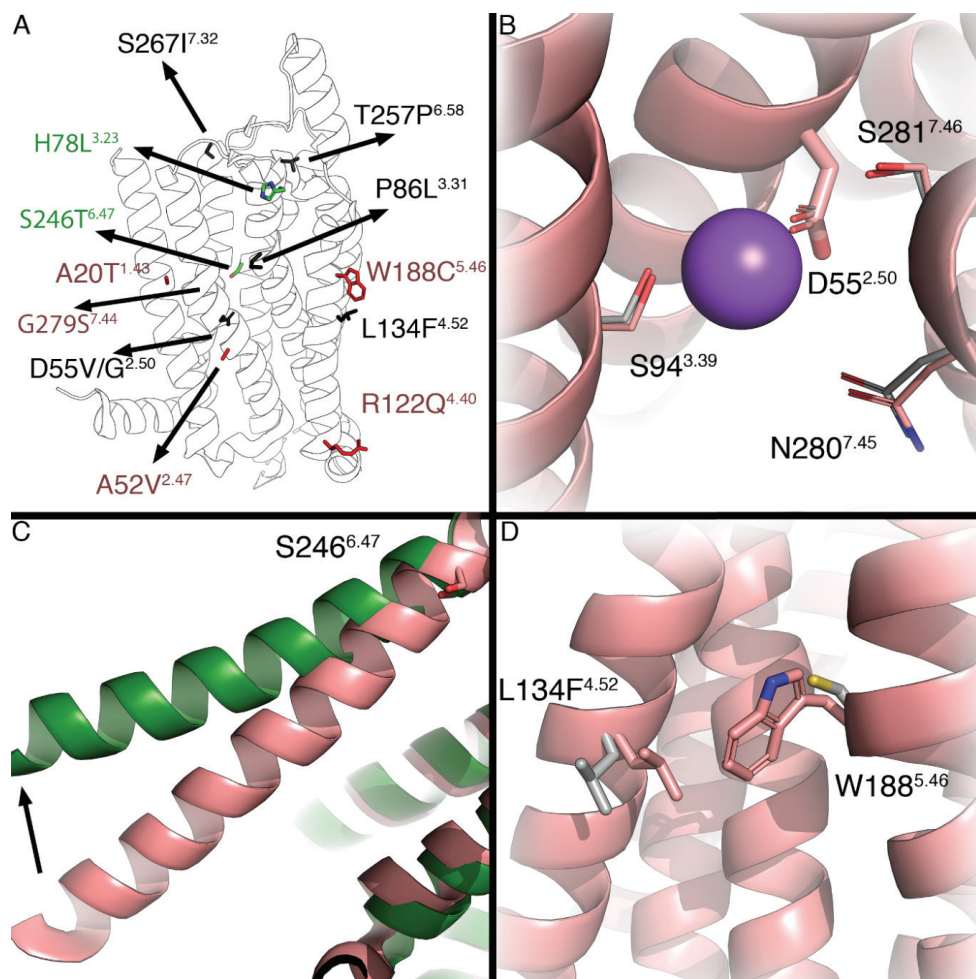
Figure 6. A) Overview of all mutations mapped on the X-ray structure of the hA$_1$AR, inactive (5UEN) in red and active (6D9H) in green. Residues are colored by their observed effect, CAMs in green, CIMs in red and LFMs in black. B) Close up of residue D55$^{2.50}$. In grey, residues that are found in the A$_{2A}$AR binding site, with the sodium ion from that structure (PDB: 4EIY) in purple. C) Residue S246$^{6.47}$ is found near the hinging region of TM6, the outward motion of which is associated with receptor activation (shown with arrow). D) Residues L134$^{4.52}$ and W188$^{5.46}$ form a cluster and are pointing toward the membrane.

It is known that ELs are essential in ligand binding and the receptor activation mechanism in class A GPCR[18]. Therefore, we hypothesize that the loss of the anionic charge hinders the salt bridge formation and stabilizes the receptor conformation in its active state.

Mutant receptors P86L$^{3.31}$, T257P$^{6.58}$ and S267I$^{7.32}$ were characterized as LFMs with complete loss of activation. Although this could be due to loss of expression (expression levels could not be determined in yeast), it had been shown in a previous study on A$_1$AR that mutant receptor P86F$^{3.31}$ resulted in abolished CPA binding. This indicates

that the proline at residue 86 indirectly affects ligand binding by re-orienting the TM1 conformation to favor N[6] substituents[39]. Both P86L[3.31] and P86F[3.31] are mutations in which the small size and rigid residue proline was exchanged by larger amino acids with hydrophobic side chains. Introduction of these larger side chains is potentially the causal factor for the loss of receptor activation. The residue T257[6.58], located at the top part of the helix 6, forms a hydrophobic pocket along with M177[5.35], L253[6.54] and T270[7.35] which has been shown to accommodate the antagonist DU172 in the A$_1$AR[32]. In A$_{2A}$AR, an alanine mutation at residue T256[6.58] has been shown to result in decreased affinity of reference antagonist ZM241385[40]. It is known that proline introduces kinks in α-helices due to the absence of an H-bond donor in addition to steric hindrance disrupting amide backbone hydrogen bond formation[41]. Therefore, in A$_1$AR, the proline mutation at T257[6.58] likely altered the receptor conformation, and resulted in loss of receptor activation. Mutant receptor S267I[7.32], located at the top of helix 7 and end of ECL3, showed a complete loss of activation in response to CPA, indicating that residue S267 may indirectly affect ligand binding.

Mutations located on conserved residues

Conserved residues and motifs of GPCRs are known to mediate ligand binding and receptor functionality[19]. Thus, mutations located at these residues may cause prominent alterations of receptor pharmacology. Alanine at residue 2.47 is highly conserved among class A GPCRs (72 %)[42]. Mutant receptor A52V[2.47] showed a dramatic decrease in both potency and efficacy of CPA (Figure 2A and Table 2), which could not be confirmed in mammalian cells due to a lack of expression. Interestingly, this same mutation occurs in CCR5, where this seemingly small change in the side chain, has been reported to greatly affect binding of CCL5[43], indicating the essential role of residue A2.47 in receptor-ligand interaction.

Two LFMs, D55G[2.50] and D55V[2.50], are found at residue D[2.50], which is the most highly conserved residue among class A GPCRs (92 %)[44]. D[2.50] together with S[3.39] regulates Na$^+$-binding[45]. Mutations at residue D[2.50] are known to alter ligand binding and/or G protein signaling[34,46]. Abolished G protein signaling has also been reported on mutant receptor D52N[2.50] in A$_{2A}$AR, in which it was shown that inter-helical packing was impacted by the change from aspartic acid to asparagine[46]. Therefore, our results implicate that the loss of the negatively charged side chain in D[2.50] impedes electrostatic interactions with Na$^+$-ions and thereby leads to decreased receptor activation.

S246[6.47] belongs to the conserved CWxP motif in helix 6, which is classified as the microswitch region and associated with receptor activation[47]. In the CWxP motif, cysteine at residue 6.47 is conserved by 71 % among class A GPCR and serine is 10 %[44]. In both yeast and mammalian systems, mutant receptor S246T[6.47] showed slightly increased potency values of CPA (Figure 2C, 5A, Table 2 and 4). The increase in potency value could be caused by the increase in ligand binding of CPA (Figure 4C). Additionally, hA$_1$AR was not locked in the active conformation by mutation

S246T[6.47], as DPCPX could still deactivate the receptor (Figure 3). Similarly, in the ß$_2$-adrenergic receptor, the mutation C285T[6.47] has been characterized as a CAM, while C285S[6.47] had similar properties to the wild-type receptor[47]. As it is known that residue 6.47 is crucial for the rotamer toggle switch[47], a threonine mutation on 6.47 may alter the side chain modulation of the rotamer toggle switch, therefore, further impacting the movement of TM6 during receptor activation.

Mutations located on residues pointing towards the membrane

In mammalian cell membranes, cholesterol has been reported to have a modulatory role in GPCR function via interaction with residues in the lipid-protein interface[48]. Moreover, compared to the membranes of mammalian cells, the yeast cell membrane contains less cholesterol and more ergosterol, which may result in a different receptor conformation, and thus functionality of human GPCRs between expression systems[48,49]. Moreover, the conflicting results obtained from different expression systems could be caused by differences in receptor expression levels.

Mutant receptor G279S[7.44] has been characterized as a CIM with retained potency and efficacy of CPA in the yeast system, while decreased constitutive activity could not be observed in the mammalian system, possibly due to the slightly higher expression level than wild-type hA$_1$AR. Interestingly, G279S[7.44] has also been identified as a Parkinson's disease-associated mutation, which did not alter receptor expression or ligand binding but influenced the heteromerization with the dopamine D$_1$ receptor[50].

Mutant receptor W188C[5.46] showed a 10-fold decrease in the potency value of CPA in both yeast and mammalian systems (Figure 2C, Figure 5A,Table 4 and Table 2). This decrease in potency was caused by the decrease in affinity of CPA (Figure 4C and Table 3). Despite the maintenance of hydrophobicity of the side chain, the substitution of tryptophan to cysteine introduced a dramatic reduction of side chain size. Reducing the amino acid side chain size at position W188[5.46] may affect the receptor-ligand interaction of CPA on hA$_1$AR. Moreover, it has been shown that W188[5.46] together with residues V137[4.55], F144[4.62], W146, Y182[5.40], F183[5.41] and V187[5.45] are part of a hydrophobic core, which along with residues S150 and R154 forms contacts with the EL2 of two A$_1$AR homodimers in mammalian cells[32]. It has been hypothesized that EL2 exerts a crucial role in the transition between G protein-coupled and -uncoupled states[51]. While it was previously suggested that A$_1$AR homodimerizes, leading to cooperative orthosteric ligand binding in mammalian cells[52], the homodimerization of A$_1$AR in yeast cells remains undetermined.

Residue L134[4.52] forms a cluster with W188[5.46] pointing towards the membrane (Figure 6D). Mutant receptor L134F[4.52] has been characterized as LFM in the yeast system. However, it behaved quite similar to wild-type A$_1$AR in the mammalian system (Figure 5 and Table 4). L134[4.52] is conserved amongst all ARs and located close to the highly conserved residue in TM4, W[4.50]. The latter is known to be involved in ligand binding and interaction with the cell membrane via cholesterol,

where complete loss of ligand binding has been observed previously by mutating tryptophan to other amino acids[48,53,54]. Phenylalanine mutation at L134[4.52] might thus indirectly change the interaction among residues W132[4.50], L99[3.44], A100[3.45], L193[5.51] and Y200[5.58 53], by the dramatic size change of the side chain, and this might be different when using a different cell membrane background.

Potential role for hA$_1$AR mutations in cancer

Activation of hA$_1$AR has been identified with anti-proliferative effects in colon cancer, glioblastoma and leukemia[10,55,56]. Mutations with inhibitory effects on receptor activation identified from colon cancer, such as the LFM D55G[2.50] and CIM W188C[5.46], might then behave as pro-proliferative regulators in cancer progression. In contrast, deletion or blockade of hA$_1$AR resulted in inhibited cell proliferation but induced PD-L1 upregulation in melanoma cells, which led to compromised anti-tumor immunity[57]. Additionally, the hA$_1$AR antagonist DPCPX shows inhibitory effects on tumor cell proliferation, migration, while promoting apoptosis[12,15]. Mutant receptors with altered binding affinity of DPCPX, namely L134F[4.52] and W188C[5.46] in this study, may thus impact the efficacy of DPCPX treatments. Of note, due to the low frequency in comparison to known driver mutations in cancer patients, these cancer-related mutations in hA$_1$AR are unlikely to be cancer-drivers[58]. However, passenger mutations should not be ruled out for in the consideration of cancer personalized therapy[59].

In conclusion, 13 cancer-induced somatic mutations located at the 7-transmembrane domain of the adenosine A$_1$ receptor were retrieved from TCGA and characterized in a robust yeast system. 2 CAMs (H78L[3.23] and S246T[6.47]), 1 LFM (L134F[4.52]) and 2 CIMs (W188C[5.46] and G279S[7.44]) were also investigated in mammalian cells. The yeast system is a suitable, rapid and accurate method for initial mutation screening that enables us to identify mutations with dramatic effect on receptor activation. However, the current study shows that this system is best used for receptor mutations on the extracellular side, ligand binding pocket or pointing inwards from the membrane. Based on the results of this study, follow-up studies in a disease-relevant system are warranted to further investigate the effect of these hA$_1$AR mutations in cell proliferation and migration, and eventually in cancer progression. Taken together, this study will enrich our understanding of the largely undefined role of hA$_1$AR in cancer progression, which may eventually improve cancer therapies.

References

1. Fredriksson, R., Lagerström, M. C., Lundin, L.-G. & Schiöth, H. B. The G-protein-coupled receptors in the human genome form five main families. Phylogenetic analysis, paralogon groups, and fingerprints. *Mol. Pharmacol.* **63**, 1256–72 (2003).
2. Vassilatis, D. K. *et al*. The G protein-coupled receptor repertoires of human and mouse. *Proc. Natl. Acad. Sci.* **100**, 4903–4908 (2003).
3. Lagerström, M. C. & Schiöth, H. B. Structural diversity of G protein-coupled receptors and significance for drug discovery. *Nat. Rev. Drug Discov.* **7**, 339–57 (2008).
4. Pierce, K. L., Premont, R. T. & Lefkowitz, R. J. Seven-transmembrane receptors. *Nat. Rev. Mol. Cell Biol.* **3**, 639–650 (2002).

5. Kan, Z. *et al.* Diverse somatic mutation patterns and pathway alterations in human cancers. *Nature* **466**, 869–73 (2010).
6. Lappano, R. & Maggiolini, M. GPCRs and cancer. *Acta Pharmacol. Sin.* **33**, 351–362 (2012).
7. Dorsam, R. T. & Gutkind, J. S. G-protein-coupled receptors and cancer. *Nat. Rev. Cancer* **7**, 79–94 (2007).
8. Gonzalez, H., Hagerling, C. & Werb, Z. Roles of the immune system in cancer: From tumor initiation to metastatic progression. *Genes Dev.* **32**, 1267–1284 (2018).
9. Vijayan, D., Young, A., Teng, M. W. L. & Smyth, M. J. Targeting immunosuppressive adenosine in cancer. *Nat. Rev. Cancer* **17**, 709–724 (2017).
10. Gessi, S., Merighi, S., Sacchetto, V., Simioni, C. & Borea, P. A. Adenosine receptors and cancer. *Biochim. Biophys. Acta* **1808**, 1400–1412 (2011).
11. Merighi, S. *et al.* A glance at adenosine receptors: novel target for antitumor therapy. *Pharmacol. Ther.* **100**, 31–48 (2003).
12. Sek, K. *et al.* Targeting Adenosine Receptor Signaling in Cancer Immunotherapy. *Int. J. Mol. Sci.* **19**, 3837 (2018).
13. Merighi, S. *et al.* Pharmacological and biochemical characterization of adenosine receptors in the human malignant melanoma A375 cell line. *Br. J. Pharmacol.* **134**, 1215–1226 (2001).
14. Borea, P. A., Gessi, S., Merighi, S., Vincenzi, F. & Varani, K. Pharmacology of Adenosine Receptors: The State of the Art. *Physiol. Rev.* **98**, 1591–1625 (2018).
15. Zhou, Y. *et al.* The Adenosine A₁ Receptor Antagonist DPCPX Inhibits Tumor Progression via the ERK/JNK Pathway in Renal Cell Carcinoma. *Cell. Physiol. Biochem.* **43**, 733–742 (2017).
16. Mirza, A. *et al.* RNA interference targeting of A₁ receptor-overexpressing breast carcinoma cells leads to diminished rates of cell proliferation and induction of apoptosis. *Cancer Biol. Ther.* **4**, 1355–1360 (2005).
17. Peeters, M. C. *et al.* The role of the second and third extracellular loops of the adenosine A₁ receptor in activation and allosteric modulation. *Biochem. Pharmacol.* **84**, 76–87 (2012).
18. Peeters, M. C., van Westen, G. J. P., Li, Q. & IJzerman, A. P. Importance of the extracellular loops in G protein-coupled receptors for ligand recognition and receptor activation. *Trends Pharmacol. Sci.* **32**, 35–42 (2011).
19. Jespers, W. *et al.* Structural mapping of adenosine receptor mutations: ligand binding and signaling mechanisms. *Trends Pharmacol. Sci.* **39**, 75–89 (2017).
20. Beukers, M. W. *et al.* Random Mutagenesis of the Human Adenosine A₂B Receptor Followed by Growth Selection in Yeast. Identification of Constitutively Active and Gain of Function Mutations. *Mol. Pharmacol.* **65**, 702–710 (2004).
21. Stewart, G. D. *et al.* Determination of adenosine A₁ receptor agonist and antagonist pharmacology using *Saccharomyces cerevisiae*: Implications for ligand screening and functional selectivity. *J. Pharmacol. Exp. Ther.* **331**, 277–286 (2009).
22. Weinstein, J. N. *et al.* The Cancer Genome Atlas Pan-Cancer analysis project. *Nat. Genet.* **45**, 1113–1120 (2013).
23. UniProt: the universal protein knowledgebase. *Nucleic Acids Res.* **45**, D158–D169 (2017).
24. Ballesteros, J. A. & Weinstein, H. Integrated methods for the construction of three-dimensional models and computational probing of structure-function relations in G protein-coupled receptors. in *Methods in Neurosciences* **25**, 366–428 (1995).
25. Isberg, V. *et al.* Generic GPCR residue numbers – aligning topology maps while minding the gaps. *Trends Pharmacol. Sci.* **36**, 22–31 (2015).
26. Dowell, S. J. & Brown, A. J. Yeast Assays for G Protein-Coupled Receptors. in *Methods in molecular biology (Clifton, N.J.)* **552**, 213–229 (Springer New York, 2009).
27. Longo, P. A., Kavran, J. M., Kim, M. S. & Leahy, D. J. Transient mammalian cell transfection with polyethylenimine (PEI). *Methods Enzymol.* **529**, 227–240 (2013).
28. Heitman, L. H. *et al.* A Series of 2,4-Disubstituted Quinolines as a New Class of Allosteric Enhancers of the Adenosine A₃ Receptor. *J. Med. Chem.* **52**, 926–931 (2009).
29. Smith, P. K. *et al.* Measurement of protein using bicinchoninic acid. *Anal. Biochem.* **150**, 76–85 (1985).
30. Schöneberg, T., Liu, J. & Wess, J. Plasma Membrane Localization and Functional Rescue of Truncated Forms of a G Protein-coupled Receptor. *J. Biol. Chem.* **270**, 18000–18006 (1995).
31. de Ligt, R. A. F., Rivkees, S. A., Lorenzen, A., Leurs, R. & IJzerman, A. P. A "locked-on," constitutively active mutant of the adenosine A₁ receptor. *Eur. J. Pharmacol.* **510**, 1–8 (2005).
32. Glukhova, A. *et al.* Structure of the Adenosine A₁ Receptor Reveals the Basis for Subtype Selectivity. *Cell* **168**, 867-877.e13 (2017).
33. Draper-Joyce, C. J. *et al.* Structure of the adenosine-bound human adenosine A₁ receptor–Gᵢ complex. *Nature* **558**, 559–563 (2018).
34. Liu, W. *et al.* Structural basis for allosteric regulation of GPCRs by sodium ions. *Science.* **337**, 232–236 (2012).
35. Esguerra, M., Siretskiy, A., Bello, X., Sallander, J. & Gutiérrez-de-Terán, H. GPCR-ModSim: A comprehensive web based solution for modeling G-protein coupled receptors. *Nucleic Acids Res.* **44**, W455–W462 (2016).
36. Cheng, Y.-C. & Prusoff, W. H. Relationship between the inhibition constant (KI) and the concentration of inhibitor which causes 50 per cent inhibition (I50) of an enzymatic reaction. *Biochem. Pharmacol.* **22**, 3099–3108 (1973).
37. Nguyen, A. T. N. *et al.* Extracellular Loop 2 of the Adenosine A₁ Receptor Has a Key Role in Orthosteric Ligand Affinity and Agonist Efficacy. *Mol. Pharmacol.* **90**, 703–714 (2016).
38. Motulsky, H. J. & Neubig, R. R. Analyzing Binding Data. *Current Protocols in Neuroscience* **52**, 7.5.1-7.5.65 (2010).
39. Rivkees, S. A., Barbhaiya, H. & IJzerman, A. P. Identification of the adenine binding site of the human A₁ adenosine receptor. *J Biol Chem* **274**, 3617–3621 (1999).
40. Guo, D. *et al.* Molecular basis of ligand dissociation from the adenosine A₂A receptor. *Mol. Pharmacol.* **89**, 485–491 (2016).
41. Chou, P. Y. & Fasman, G. D. Secondary structural prediction of proteins from their amino acid sequence. *Trends in Biochemical Sciences.* **2**, 128-131 (1977).
42. Isberg, V. *et al.* GPCRdb: an information system for G protein-coupled receptors. *Nucleic Acids Res.* **44**, D356–D364 (2016).
43. Howard, O. M. Z. *et al.* Naturally occurring CCR5 extracellular and transmembrane domain variants affect HIV-1 co-receptor and ligand binding function. *J. Biol. Chem.* **274**, 16228–16234 (1999).
44. Katritch, V. *et al.* Allosteric sodium in class A GPCR signaling. *Trends Biochem Sci* **39**, 233–244 (2014).
45. Barbhaiya, H., McClain, R., IJzerman, A. & Rivkees, S. A. Site-directed mutagenesis of the human A₁ adenosine receptor: influences of acidic and hydroxy residues in the first four transmembrane domains on ligand binding. *Mol. Pharmacol.* **50**, 1635–42 (1996).
46. White, K. L. *et al.* Structural Connection between Activation Microswitch and Allosteric Sodium Site in GPCR Signaling. *Structure* **26**, 259-269.e5 (2018).
47. Shi, L. *et al.* β₂ adrenergic receptor activation: Modulation of the proline kink in transmembrane 6 by a rotamer toggle switch. *J. Biol. Chem.* **277**, 40989–40996 (2002).
48. Paila, Y. D., Tiwari, S. & Chattopadhyay, A. Are specific nonannular cholesterol binding sites present in G-protein

coupled receptors? *Biochim. Biophys. Acta - Biomembr.* **1788**, 295–302 (2009).

49. Elkins, M. R., Sergeyev, I. V. & Hong, M. Determining Cholesterol Binding to Membrane Proteins by Cholesterol 13C Labeling in Yeast and Dynamic Nuclear Polarization NMR. *J. Am. Chem. Soc.* **140**, 15437–15449 (2018).

50. Nasrollahi-Shirazi, S. *et al.* Functional impact of the G279S substitution in the adenosine A$_1$-receptor (A$_1$R-G279S[7.44]), a mutation associated with Parkinson's disease. *Mol. Pharmacol.* **98**, 250-266 (2020).

51. Bokoch, M. P. *et al.* Ligand-specific regulation of the extracellular surface of a G-protein-coupled receptor. *Nature* **463**, 108–112 (2010).

52. Gracia, E. *et al.* Homodimerization of adenosine A$_1$ receptors in brain cortex explains the biphasic effects of caffeine. *Neuropharmacology* **71**, 56–69 (2013).

53. Suzuki, T. *et al.* A highly conserved tryptophan residue in the fourth transmembrane domain of the A$_1$ adenosine receptor is essential for ligand binding but not receptor homodimerization. *J. Neurochem.* **110**, 1352–1362 (2009).

54. Rhee, M. H., Nevo, I., Bayewitch, M. L., Zagoory, O. & Vogel, Z. Functional role of tryptophan residues in the fourth transmembrane domain of the CB2 cannabinoid receptor. *J. Neurochem.* **75**, 2485–2491 (2000).

55. Saito, M., Yaguchi, T., Yasuda, Y., Nakano, T. & Nishizaki, T. Adenosine suppresses CW2 human colonic cancer growth by inducing apoptosis via A$_1$ adenosine receptors. *Cancer Lett.* **290**, 211–215 (2010).

56. Lan, B. *et al.* Metformin suppresses CRC growth by inducing apoptosis via ADORA1. *Front. Biosci. - Landmark* **22**, 248–257 (2017).

57. Liu, H. *et al.* ADORA1 Inhibition Promotes Tumor Immune Evasion by Regulating the ATF3-PD-L1 Axis. *Cancer Cell* **37**, 324-339.e8 (2020).

58. Gimm, O. *et al.* Over-representation of a germline RET sequence variant in patients with sporadic medullary thyroid carcinoma and somatic RET codon 918 mutation. *Oncogene* **18**, 1369–1373 (1999).

59. Monticelli, M. *et al.* Passenger mutations as a target for the personalized therapy of cancer. *PeerJ* **Preprints**, (2018).

6